An efficient optimisation tool for floating offshore wind support structures

Energy Reports 8 (2022) 9104–9118

Contents lists available at ScienceDirect

Energy Reports

journal homepage: www.elsevier.com/locate/egyr

Research paper

An efficient optimisation tool for floating offshore wind support structures

E. Faraggiana *, M. Sirigu, A. Ghigo, G. Bracco, G. Mattiazzo

Department of Mechanical and Aerospace Engineering, Polytechnic University of Turin, 10129 Torino, Italy

ARTICLE INFO

Article history:
Received 1 March 2022
Received in revised form 21 June 2022
Accepted 8 July 2022
Available online xxxx

Keywords:
Renewable energy
Wind turbine
Offshore
Floating platform
Optimisation

ABSTRACT

Floating offshore wind turbines (FOWTs) are a rapidly developing technology, but still, need to gain economic competitiveness to obtain market acceptance. The reduction of the structural cost of the floating platform represents one of the main targets to reach an optimal design in the initial design process. This paper proposes an efficient optimisation tool that could be applied to any floating wind turbine to optimise the main geometry design parameters. In this study, the OC3 spar buoy concept is considered as an example, where the stability and dynamic performance of the device are verified using hydrostatic and time-domain computations. The numerical simulations are solved using an in-house MATLAB code that uses Salome-Meca to create the mesh and obtain hydrostatic and dynamic properties of the platform, Nemoh to calculate the hydrodynamic coefficients and an aero-hydro-servo Simscape model for the time-domain simulation. The main geometry design parameters of the buoy are optimised using a genetic algorithm in combination with the Kriging surrogate model to minimise the buoy's structural cost while ensuring the spar's performance. The optimal design reduces the cost by two to three times the worst configuration of the design space and there is also a 25% cost reduction between the most and the least restrictive optimal cases. The optimal design results demonstrate the hydrostatic constraints' significance over the dynamic ones as they mostly influence the feasible design area. However, the results of this work could only be specific to the design case considered, and careful consideration should be given to other types of geometries. The optimisation approach presented is particularly important as it is flexible and can be adapted to other platforms.

1. Introduction

Offshore wind energy is expected to play an important role in EU energy policy (EU-OEA, 2010). Floating wind turbines can be deployed in larger water depths, where higher wind speeds are reached compared to onshore wind and fixed offshore wind turbines (Esteban et al., 2011). In addition, floating wind farms can be deployed in larger suitable free areas. The design of the floating support structure is still a major challenge for the industrialisation of this technology, for which many concepts have already been developed (Galván et al., 2018; Roddier et al., 2010; Ahn and Shin, 2019; Engineering, 2021). The size and weight of the platform still have great potential in terms of optimal design and cost reduction. In fact, the cost could still be reduced by 16%, as shown in James and Ros (2015). In Fylling and Berthelsen (2011), a design tool for optimising the support structure of a spar concept was presented. This optimisation tool optimised the spar geometry, the mooring attachment points and the diameter of the damper plate to minimise the cost of the device. It considered various design constraints such as tower pitch and nacelle acceleration. However, this tool simplified the rotor aerodynamics and did not consider the effects of wind turbine control. An extended investigation of the platform geometry, including semi-submersible, spar and TLP was addressed in Hall et al. (2013), Karimi et al. (2017). These studies included the wind turbine effects using an aerodynamic stiffness and damping matrices computed from FAST (National Renewable Energy Laboratory, 2021) but were limited to frequency-domain analysis. A multi-objective system GA was used to minimise both structural costs and nacelle acceleration. Time-domain analysis to optimise the floating support concept is limited to only a few works as they are generally more computationally expensive (Myhr and Nygaard, 2012; Lee et al., 2015; Leimeister et al., 2020). However, they have the advantage accounting for non-linear effects, and are therefore more accurate than frequency-domain models. In this perspective, this paper considers hydrostatic and time-domain analysis to optimise the structural costs derived from investigating the geometry of the OC3 Spar type floating offshore wind

* Corresponding author.
E-mail addresses: emilio.faraggiana@polito.it (E. Faraggiana), massimo.sirigu@polito.it (M. Sirigu), alberto.ghigo@polito.it (A. Ghigo), giovanni.bracco@polito.it (G. Bracco), giuliana.mattiazzo@polito.it (G. Mattiazzo).

https://doi.org/10.1016/j.egyr.2022.07.036

Table 1
Properties of the OC3 floating wind turbine system (Jonkman, 2010; Jonkman et al., 2009).

Mooring system	Number of mooring lines	3
	Anchor depth, radius from centreline (m)	320, 853.87
	Fairlead depth, radius from centreline (m)	70, 5.2
	Unstretched mooring line length, diameter (m)	902.2, 0.09
	Total vertical preload (MN)	1.607
Tower	Base, top elevations (m)	10, 87.6
	Base, top diameters (m)	6.5, 3.87
	Mass (kg)	249718
Rotor-nacelle	Rotor diameter (m)	126
	Hub height (m)	90
	Mass (kg)	350000

(a) (b)

Fig. 1. Towing (a) and operating condition (b) of the Hywind spar (offshoreWIND.biz, 2017; Renewables Now, 2019).

turbine (Jonkman, 2010) for the Pantelleria case study. The OC3 spar is chosen as an example to test our optimisation tool. The geometry is simple compared to other platforms, so it is a good first choice for our tool. We do not believe that the spar is the most viable platform solution as it requires higher foundation, transportation, and installation costs than the semi-submersible type, which can also be used in shallower water depths. This tool is very flexible to optimise the design geometry parameters of any platform. Therefore, in further studies, other types of platforms can be considered and compared.

This work first deals with the computation of the hydrostatic properties such as the metacentric height and the static pitch angle which are limited to some constraints. Then, an efficient time-domain computation based on look-up tables of the aerodynamic and mooring loads, which are particularly suitable for an optimisation process, is used to verify the satisfaction of the dynamic constraints such as the nacelle acceleration and the platform pitch angle. The optimal design results of the spar are investigated for different hydrostatic and dynamic constraint values and are compared between hydrostatic and dynamic design optimisations. This study shows the importance of the hydrostatic constraints over the dynamic ones and gives some confidence in structural design optimisations based on hydrostatic constraints only. The optimisation approach is based on open-source software apart MATLAB, which makes this methodology particularly suitable for research development. The methodology is also particularly flexible for other types of platforms which makes this tool very effective. This design case study was selected as an application study for its simplicity and will be further developed to include fatigue analysis and a larger number of design variables.

This paper first describes the floating wind turbine system analysed in Section 2.1. The optimisation approach is presented in Section 2.2 and the hydrostatic and dynamic modules in Sections 2.3 and 2.4. Section 2.5 shows the design load cases identified for the Pantelleria case study. Section 3 presents the results of the optimisation and gives some recommendations for the optimal design of the spar. Finally, the discussion and conclusion are given in Sections 4 and 5.

2. Material and methods

2.1. Design of the floating wind turbine system

The OC3 spar buoy (Jonkman, 2010) has been chosen as a reference case for this work. The spar consists of two cylinders of different radius connected by a tapered part. The lower cylinder is the longest and could be considered in an optimisation process by varying its radius and height. Some ballast is also added to the bottom part of the lower cylinder to increase static and dynamic stability. A three-bladed 5 MW wind turbine is also attached above the floating platform. The main parameters of the OC3 wind turbine system are summarised in Table 1, and a detailed description can be found in Jonkman et al. (2009).

The design of a floating wind turbine involves detailed planning of all the operations that will occur during the lifetime of the device. The floater is generally towed out horizontally which is in a safe and stable position as shown in Fig. 1 and then upended out at sea. The floating foundation must ensure the floating stability of the wind turbine, especially during operating conditions when optimising the design.

The design of the floater considers the OC3 floater as the initial geometry from which various design variables are identified and selected. The height and radius of the float's lower cylinder (Hspar, Rspar) were chosen as optimising design variables. In fact, the lower cylindrical part mostly influences the floating platform's structure cost, as it is the largest compared to the conical and upper cylindrical parts. The other dimensions were kept the same as those of the OC3 spar and are shown in Fig. 2. The design parameters of the float specific to this study are shown in Table 2. The total weight of the steel was estimated considering

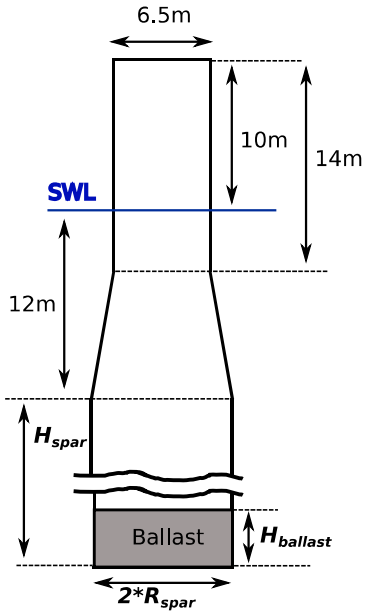

Fig. 2. Design scheme of the floater.

Table 2
Properties of the floater used in this work.

Floater	Shell material, density $\left(\frac{kg}{m^3}\right)$	Steel, 8500
	Ballast material, density $\left(\frac{kg}{m^3}\right)$	Concrete, 3000
	Shell thickness (m)	0.07
	H_{spar} design range (m)	[80 250]
	R_{spar} design range (m)	[3.25 7]

a constant thickness of the platform walls of 7 cm. The platform is ballasted with concrete at the bottom of the lower cylindrical part of the floater because the cost is lower compared to steel, and the density is about three times that of water. However, other cheaper alternatives such as a mix of gravel and water, sand, black slag and ore steel could be also good solutions, but this study does not investigate the choice of ballast material. The ballast fills a cylindrical volume that has the same inner radius of the spar. The height can be calculated imposing the hydrostatic balance of the spar considering the total vertical preload from the mooring lines (F_{mz}):

$$\begin{cases} F_{mz} = (B_F - (M_{WT} + M_F)) \cdot g \\ M_F = M_{FS} + M_{FC} \\ M_{FC} = \pi \cdot R_B^2 \cdot H_B \end{cases} \quad (1)$$

where M_{WT} is the total mass of the wind turbine system not including the floater, M_F and B_F are the mass and buoyancy of the floater, M_{FS} and M_{FC} are the steel and concrete masses of the floater, R_B and H_B are the radius and height of the ballast. The same total vertical preload from the mooring lines of the OC3 reference study is used in this work.

2.2. Optimisation approach

The main objective of the optimisation is to obtain an optimal design of the floating platform that minimises the structural cost respecting the required hydrostatic and dynamic stability (see Fig. 5). The objective function only considers the material costs required for the manufacturing process of the floating substructure. The objective function (f_{cost}) can be expressed as

$$f_{cost} = m_{struct} \cdot c_{struct} + m_{ballast} \cdot c_{ballast} \quad (2)$$

Table 3
Material properties and specific costs of the floating platform (INNWIND.EU, 2014).

	Material	Density (kg/m^3)	Specific cost (€/ton)
Structure	Steel	8500	3000
Ballast	Concrete	3000	500

where m_{struct} and $m_{ballast}$ are the masses of the structure and the ballast while c_{struct} and $c_{ballast}$ are the specific costs associated to the material. In this study, the structure is made of steel with a thickness of 7 cm, similar to that chosen in the Innwind deliverable (INNWIND.EU, 2014). A summary of the material density and cost is given in Table 3.

The optimisation methodology includes two main modules, the hydrostatic module and the dynamic module, as described in Fig. 5. The simulation of the different modules is used to estimate the steel and concrete mass required for the objective function and to verify the design constraints. The hydrostatic constraints are the static pitch angle and the metacentric height while the dynamic constraints are the maximum dynamic pitch angle of the platform and the root mean square (rms) value of the nacelle acceleration. Most of the constraints relate to the floating stability of the system. The nacelle acceleration is also considered to account for fatigue analysis effects as it is responsible of the stress on the blades and drivetrain of the wind turbine which reduces the turbine's lifetime. For the optimisation module, it is very important that each simulation run is completely parametrised as a function of the design parameters. For this purpose, Salome-Meca (Codeaster, 2019) was chosen because it is open-source and allows a Text User Interface (TUI) based in Python, through which the geometry parameters are automatically parametrised. Essential material properties for the optimisation module such as the steel mass, the displaced volume, the Centre Of Gravity (COG) and the mesh of the platform were obtained from Salome-Meca. The mass of the ballast required to estimate the objective function is then computed using Eq. (1). In-house code based in MATLAB is also used to compute the curve of statical stability and the wind load of the wind turbine to estimate the static pitch angle and the metacentric height. These quantities are compared with the constraints and a penalty function is given for the design solutions that do not respect the limits. In the same way, the dynamic module also assigns a penalty function if the dynamic stability constraints are not met. The penalty functions are chosen to replace the objective function as large constant values when the constraints are violated (30–31 M €). The mesh and the COG of the floating platform computed in Salome-Meca are used to obtain the hydrodynamic coefficients from Nemoh (Babarit, 2017), an open-source Boundary Element Method (BEM) solver based on a linear potential flow theory. The hydrodynamic coefficients are crucial for the time-domain model used in this work, as the hydrodynamic loads are important to assess the dynamic motion of the floater. There are other fundamental loads that the floating wind turbine must take into account, namely the aerodynamic and mooring loads. Furthermore, the control system should be included to simulate the real operating conditions of a commercial wind turbine, where power is maximised and limited by the rated power. These dynamic effects are included in the model and will be described in detail in the next sections. The dynamic simulation is performed in a Simulink/Simscape environment (MathWorks, 2022b) and uses the WEC-Sim library, a powerful open-source tool for simulating floating bodies (Ruehl et al., 2020; Tethys, 2022).

An efficient global free-gradient optimisation algorithm is chosen to reduce as much as possible the number of simulations required to achieve convergence to the optimal design (Fig. 3).

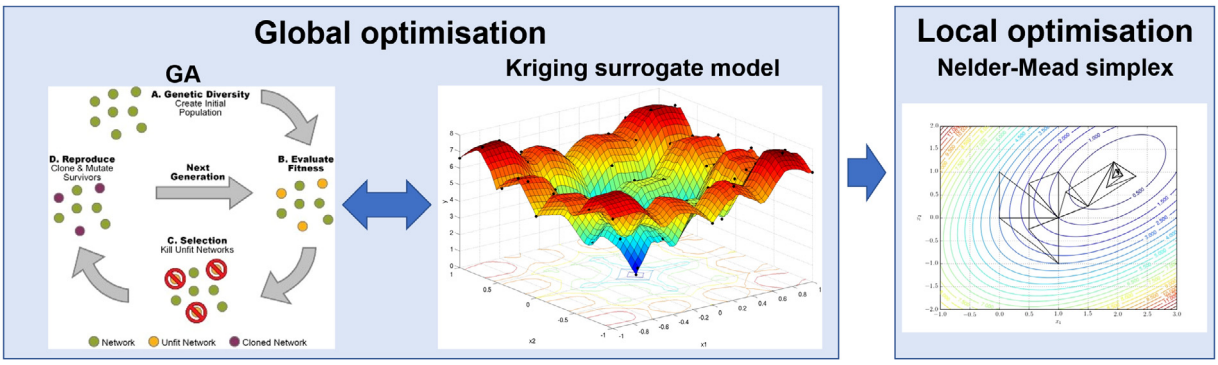

Fig. 3. The optimisation algorithm chosen in the study (Ghent University, 2022; QuantDare, 2022; Sachin Joglekar's blog, 2022).

The optimisation first searches for the region of the global optimum using stochastic optimisation and then refines the optimum using deterministic optimisation. This methodology was also recommended in Cavazzuti (2012). Stochastic optimisation generally consists of a meta-heuristic algorithm such as the evolutionary algorithm, particle swarm and simulated annealing. The meta-heuristic optimisation algorithm used in this study combines the Genetic Algorithm (GA) and the Kriging surrogate model, which has shown faster convergence to the optimum compared to using GA alone (Faraggiana et al., 2020). The Kriging surrogate model is used to build a regression model from the numerical model simulations and is used to generate new individuals in the population of GA using an elitism factor. The MATLAB function "fminsearch", which uses the Nelder–Mead simplex algorithm, is used in the last part of the optimisation because of its higher convergence efficiency. The optimisation parameters are listed in Table 4. The population of each new generation of the genetic algorithm consists of 10% (elitism factor) of the best individuals calculated by the surrogate model. In particular, the surrogate model estimates the performance of 100·gen_i individuals distributed in the design space with a Latin Hypercube Design of Experiment (DoE), where gen_i is the current generation during GA. During the simulation of the optimisation algorithm the surrogate model is created from a larger number of solutions in each new generation and is therefore more accurate. So it is possible to consider a larger number of individuals for the selection of the best individual of the surrogate model during the optimisation process.

The main advantage of combining the genetic algorithm with the surrogate model is the increase in efficiency of the algorithm compared to the genetic algorithm alone. In fact, the computational time required by the surrogate model is negligible compared to that for the entire simulation of a configuration (1–2 s versus 2–5 min). Thus, the higher efficiency of GA +surrogate reduces the total computational time required to obtain the optimal design solution. The performance of the modified GA, which includes the surrogate model, has been investigated in previous work, such as in Faraggiana et al. (2020). Several changes were made compared to the original GA code, such as the memory of previous individuals, tuning of crossover and mutation probability and population during GA computation. However, in this work, only the memory of previous individuals and the surrogate model are considered. Individuals already calculated in previous generations are replaced in the new generation by new individuals next to the best minimum found, as explained in Faraggiana et al. (2020). The efficiency of GA considering the surrogate (50% elitism factor) compared to GA alone, which includes both the memory of previous individuals, is examined for the Rosenbrock function (Kok and Sandrock, 2009) in Fig. 4. The results of the algorithm show a large variability due to its stochastic nature and are therefore the average of 100 different optimisations.

Table 4
The optimisation parameters used in the algorithm.

Population	20
Generations	7
Crossover probability	0.9
Mutation probability	0.1
Elitism factor	0.1
Fminsearch simulations	10

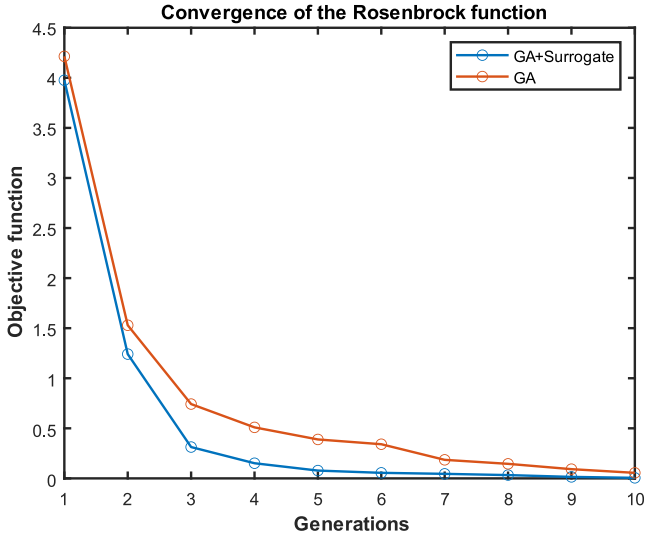

Fig. 4. The convergence of the Rosenbrock function for the GA+Surrogate and GA.

2.3. Hydrostatic module

The hydrostatic module is used to assess the hydrostatic stability, which is fundamental for the deployment of the floating wind turbine system. The initial stability can first be evaluated by calculating the metacentre. The floating structure is hydrostatically stable if the metacentre is above the centre of gravity. In general, the standard prescribes a certain positive metacentric height (GM) (DNV-GL, 2018). The metacentric height can be expressed as a function of the metacentric radius (BM):

$$GM = KB + BM - KG = KB + \frac{I}{V} - KG \tag{3}$$

where K is the origin of the vertical coordinates, B and G are the center of buoyancy and gravity, I is the moment of inertia of the waterplane about the axis of inclination, V is the volume of displacement.

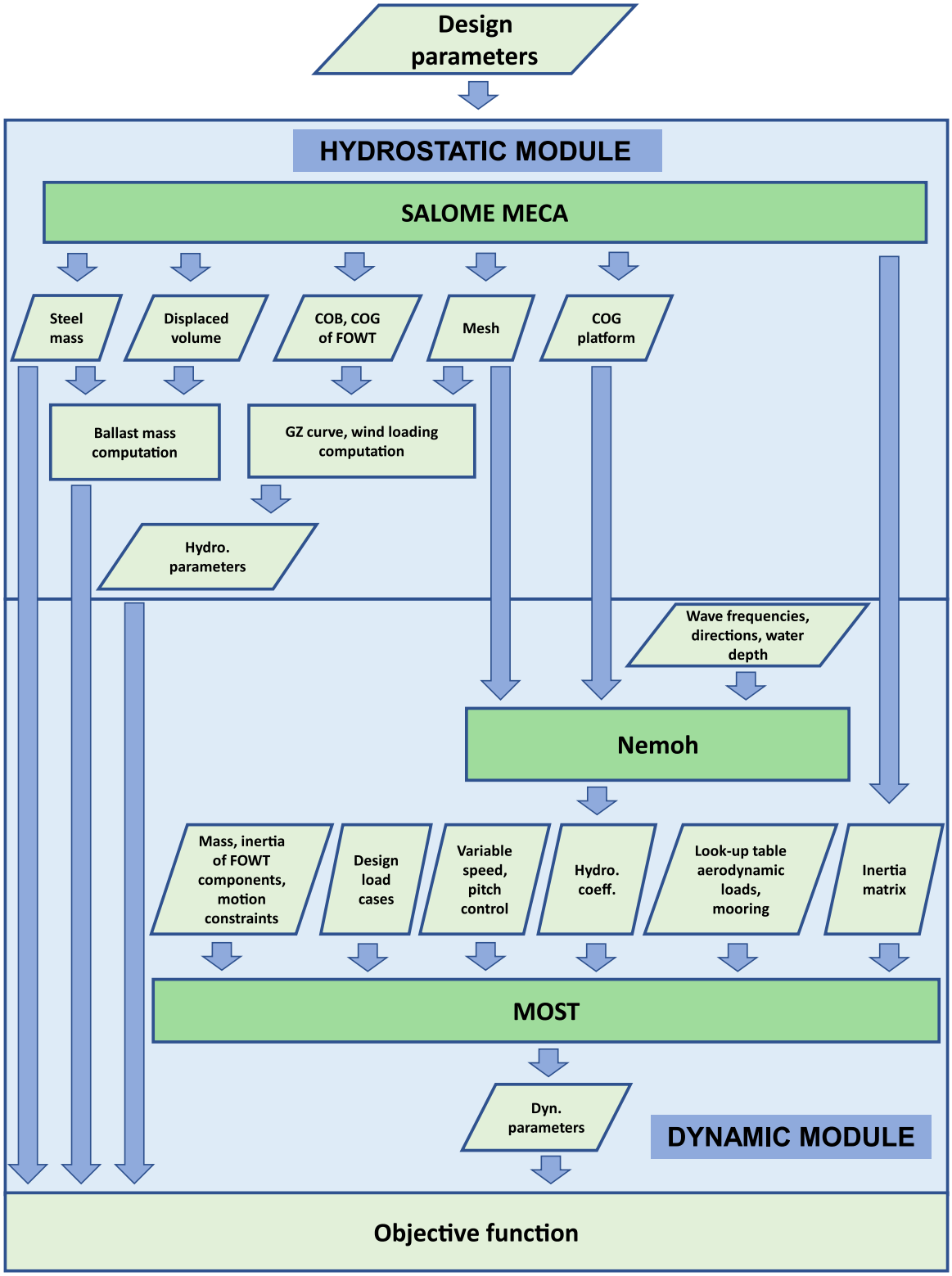

Fig. 5. The optimisation module for a floating offshore wind turbine.

The angle of statical equilibrium of the wind turbine (α_{st}) can be computed defining the hydrostatic stiffness (k_h) and the heeling moment on the wind turbine (M_h). It can be calculated as

$$\alpha_{st} = \frac{M_h}{k_h} \tag{4}$$

The hydrostatic stiffness can be expressed as

$$k_h = \rho \cdot g \cdot V \cdot GM \tag{5}$$

while the heeling moment of the wind turbine can be estimated as

$$M_h = M_{ht} + M_{hr} = \frac{1}{2}\rho_{air}\left(\int_{hmin}^{hmax} c_{Dt}\, v\,(h)^2\, D\,(h)\, hdh + c_{Tmax} V_r^2\, Ah_r\right) \cdot \cos(\alpha_h) \tag{6}$$

where M_{ht} and M_{hr} are the heeling moments due to the tower and the rotor, ρ_{air} is the air density, c_{Dt} is the drag coefficient of the tower, $v(h)$ is the logarithmic wind speed profile, *hmin* and *hmax* are the vertical distance between the center of buoyancy (COB) and the bottom and top positions of the tower, c_{Tmax} and V_r are the maximum thrust coefficient and the wind speed associated at the rotor level, A is the swept area of the rotor, h_r is the rotor height relative to the COB and α_h is the heeling angle. A more accurate assessment of hydrostatic stability could also take into account the restoring forces of the mooring lines. However, a more precise calculation of the wind heeling arm (h_r) must take into account the distance between the rotor and the mooring fairlead attachment points.

These hydrostatic properties are limited to small heeling angles, but are considered sufficient to assess the hydrostatic stability of a spar according to DNV standard (DNV-GL, 2018). These properties can be derived from the curve of statical stability after first obtaining the Salome-Meca mesh.

2.3.1. Salome-Meca

Salome-Meca is used to obtain the mesh of the spar as a function of the design parameters. A Python script is automatically generated to define the geometry and calculate the mesh. Two different meshes are generated to obtain both the curve of statical stability and to calculate the hydrodynamic coefficients from Nemoh. The computation of the hydrodynamic coefficients is more computationally expensive than the curve of statical stability and therefore a coarser mesh is required for an optimisation design process where computational efficiency is crucial. Both meshes are generated using the Netgen algorithm and triangular panels. An example of a mesh generated for the computation of the curve of statical stability is given in Fig. 6. The mesh panels are mostly regular and have a very good aspect ratio. Only the conical part has more irregular triangular shapes but the aspect ratio is still reasonable.

2.3.2. Curve of statical stability

The curve of statical stability give information about the righting moment (M_R) that can be expressed as

$$M_R = \rho_w g V GZ \tag{7}$$

where ρ_w is the water density and GZ is the righting arm. For small heel angles GZ can be expressed as

$$GZ = GM \sin(\alpha_h) \tag{8}$$

The hydrostatic force (F_H) and the righting moment are calculated from the hydrostatic pressures on the mesh given from Salome-Meca:

$$\vec{F_H} = \sum_{ip=1}^{iN} \rho_w g z_i \vec{A}_{ip} \tag{9}$$

$$\vec{M_R} = \sum_{ip=1}^{iN} (\rho_w g z_i \vec{A}_{ip}) \times \vec{D}_{ipG} \tag{10}$$

where $\vec{A}_{ip}$ is the panel area vector and $\vec{D}_{ipG}$ is the vector connecting the centre of the panel and the COG.

The heeling righting moment is determined for each heeling angle such that the design displaced volume of Salome-Meca is reached and the trim righting torque is equal to 0. However, the displaced volume and trim torque area are not known until Eq. (8) is calculated. Therefore, the optimisation algorithm fminsearch was used to obtain both the designed displaced volume and a null trim moment modifying the sinkage and the trim angles of the floating structure, respectively. In particular, the COG is updated for each sinkage, heel and trim angles.

2.4. Dynamic module

The dynamic module is used to assess the dynamic stability of the floating wind turbine system. The in-house aero-hydro-servo model MOST, which is based in Simscape, is used to simulate the OC3 spar in 6 degrees of freedom. The simulation is performed in the time-domain for 3800 s, including 200 s ramp time for transient loads. The timestep of the simulation is 0.05 s and the numerical solver is the MATLAB ode4 (MathWorks, 2022a), which uses the Runge–Kutta method. The computational time required is about 2–5 min for the computation of the hydrodynamic coefficients in Nemoh and 30 s for the time-domain simulation in MOST. The loads acting on the floating wind turbine system are described in the next sections.

2.4.1. Hydrodynamics

The frequency-domain hydrodynamic coefficients are determined using a linear potential flow theory which considers an inviscid, irrotational and incompressible fluid. Other assumptions are small wave amplitudes compared to the wavelength and small motions of the body compared to its characteristic dimensions. Nemoh is a Boundary Element Method (BEM) solver that applies Green's function to solve the radiation and diffraction problems. Nemoh was chosen because it is open-source and can be easily integrated into the optimisation design process. Convergence for some of the hydrodynamic coefficients and three different meshes is shown in Fig. 7, while details on the number of nodes and panels are given in Table 5. Fig. 7 shows very good convergence of the hydrodynamic coefficients with very little difference between them. The minimum and maximum size of the panels of the coarse mesh are chosen as reference values for the generation of the meshes dependent on the design parameters.

The time-domain hydrodynamic forces can be determined from the frequency-domain radiation and excitation coefficients using the appropriate expressions. The radiation force is obtained from the convolution integral formulation, while the excitation force expression is used for irregular waves. Further details can be found in the theory manual of WEC-Sim (Ruehl et al., 2020).

The effect of fluid viscosity is accounted in time-domain using a quadratic relationship with the fluid velocity ($\vec{v}$):

$$\vec{F_v} = -0.5\, C_d \rho_w A_d \vec{v} |\vec{v}| \tag{11}$$

where F_v is the viscous force, C_d is the drag coefficient, A_d is the characteristic area due to the drag calculation. The drag coefficient is assumed equal to 1 which is a reasonable value for long cylinders as shown in Yunus (2010).

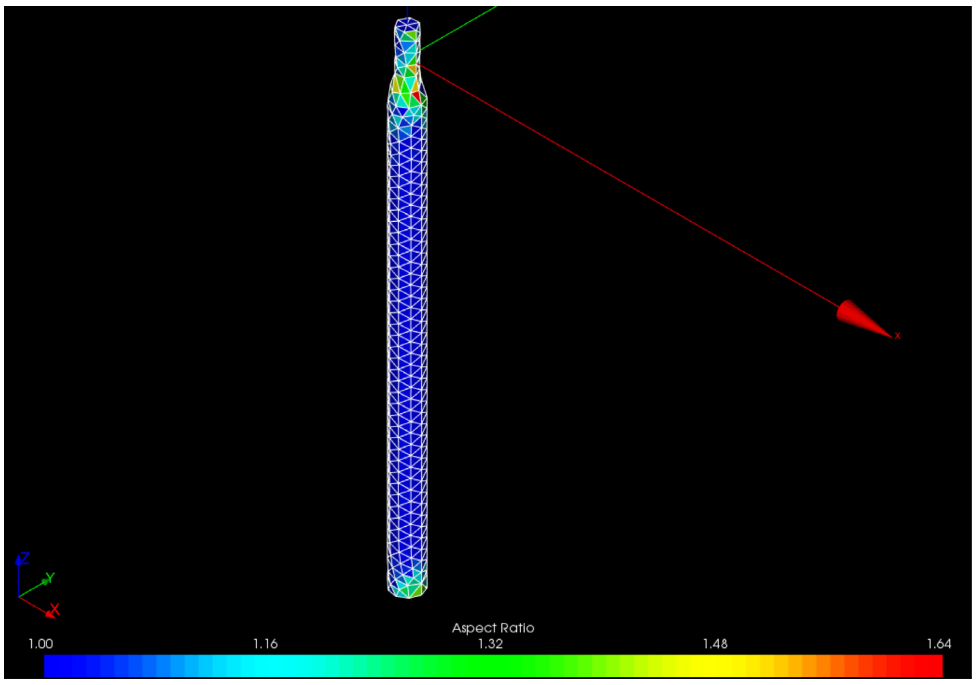

Fig. 6. The aspect ratio of the mesh generated in Salome-Meca for the calculation of the curve of statical stability.

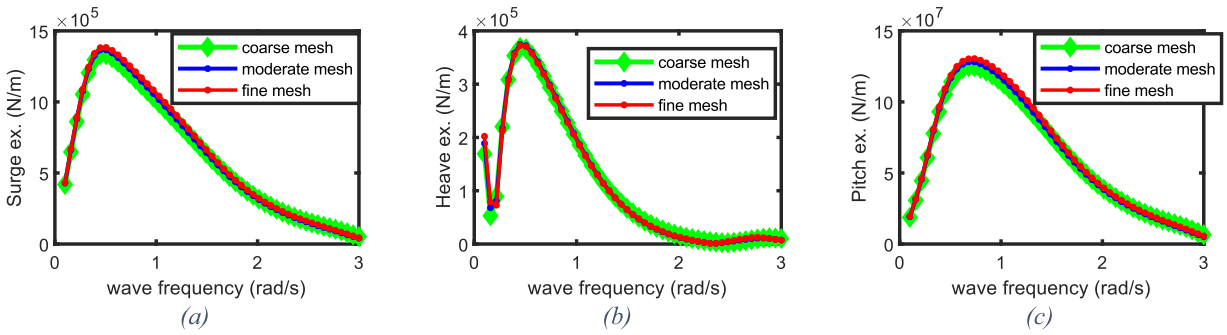

Fig. 7. The hydrodynamic convergence of the excitation coefficients for the coarse, moderate and fine meshes.

Table 5
Mesh details of the coarse, moderate and fine meshes.

	Nodes	Faces	Min. size panels	Max. size panels
Coarse	295	583	4	7
Moderate	452	896	3.5	6
Fine	646	1283	3	5.5

Table 6
Look-up table properties for the mooring loads.

	Min	Max	Step
Surge (m)	−40	40	5
Heave (m)	−10	10	5
Pitch (deg)	−10	10	5

2.4.2. Mooring

The mooring is modelled using a quasi-static approach, similar to MAP++ (Masciola, 2018) and using the same mooring line properties of the OC3 spar buoy shown in Table 1. An in-house model that computes the catenary equation for each single line is used in a similar way to Masciola et al. (2013). Each mooring line load is then applied to the attachment point of the mooring on the platform, from which the total mooring load can be obtained. A look-up table relating the total mooring load to the displacement and rotation of the platform is created to reduce computational time during the optimisation. More specifically, the total mooring load is determined as a function of the main degrees of motion of the platform, i.e. surge, heave and pitch, which are discretised as shown in Table 6. Fig. 8 shows some examples of the total mooring load computed for different surge, heave and pitch. The surge force is mostly sensitive to surge displacement, the heave force to heave while the pitch moment both to pitch and surge. The surge force is the most nonlinear compared to the heave force and pitch moment. The total mooring load computed with the platform in its origin position corresponds to a single force in heave of −1.607 MN, which is the same value given in the reference OC3 spar (Masciola et al., 2013).

2.4.3. Aerodynamics and control

The aerodynamic loads are computed using Blade Element Momentum theory (BEM) with Prandtl's tip loss and Glauert corrections. The aerodynamic loads are determined as look-up tables to reduce simulation time, as shown in Fig. 10 and Table 8. Both torque and thrust are discretised as a function of blade pitch, generator speed and wind speed alongside steady states to reduce the number of points required for discretisation and exclude those that are never reached under operating conditions.

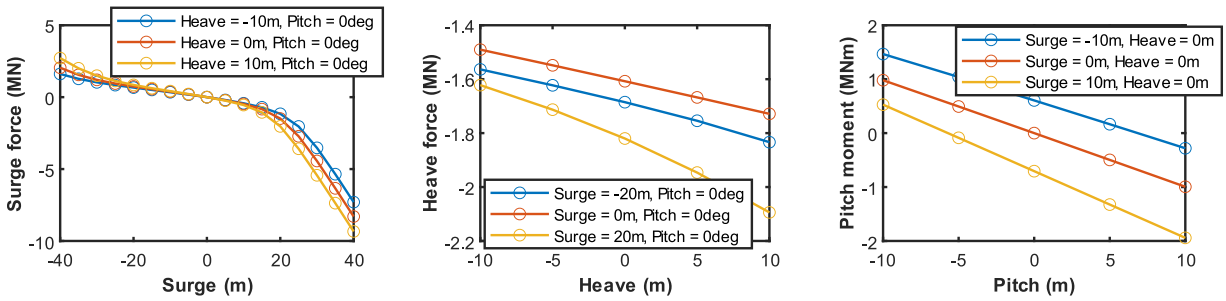

Fig. 8. Surge, heave and pitch mooring loads as a function of surge, heave and pitch motion of the platform.

Table 7
Baseline control properties.

K_P	0.006275604 s
K_I	0.0008965149
θ_k	6.302336 deg
$\frac{\partial P}{\partial \theta}$	−25.52 * 10^6 W/rad
Blade-pitch rate	8 deg/s
Minimum and maximum pitch settings	0 e 90 deg

The wind speed is also discretised with more values around the maximum thrust load conditions as it is more sensitive in this region. Fig. 10 shows the aerodynamic thrust and torque as a function of rotor speed and wind speed for the steady-state blade pitch angle. Each coloured line represents the thrust and torque for one wind speed value and for different rotor speed values. Above rated speed conditions, there is a constant torque as a function of the steady-state blade pitch angle, as required for a constant rated power. The thrust reaches a maximum value around the rated wind speed. The steady-state values for rotor speed and blade pitch are shown in Fig. 11.

Variable speed and variable pitch control are used to optimise the power generated. A look-up table that relates the generator torque and the rotor speed is used below the rated wind speed as shown in Fig. 9 and it follows the specifications given in Jonkman (2010), Jonkman et al. (2009). In particular, Region 3 gives a constant generator torque instead of a constant generator power to improve the stability of the floating system, as explained in Jonkman (2010). Above the rated wind speed, a proportional–integral (PI) control on the generator speed error. Baseline control properties are the same as those of the OC3 reference floating turbine (Jonkman, 2010) and are given in Table 7. θ_k is the blade pitch angle at which the pitch sensitivity $\left(\frac{\partial P}{\partial \theta}\right)$ is twice that at the rated operating point (θ_k). The control gains (K_P and K_I) can be expressed as

$$K_P = \frac{2 I_{Drivetrain} \Omega_0 \xi_\varphi \omega_{\varphi n}}{N_{Gear}[-\frac{\partial P}{\partial \theta}(\theta = 0)]} \tag{12}$$

$$K_I = \frac{2 I_{Drivetrain} \Omega_0 \omega_{\varphi n}^2}{N_{Gear}[-\frac{\partial P}{\partial \theta}(\theta = 0)]} \tag{13}$$

where $I_{Drivetrain}$ is the inertia of the drivetrain, Ω_0 is the rotor speed, $\omega_{\varphi n}$ and ξ_φ are the natural frequency and the damping ratio, N_{Gear} is the gearbox ratio.

2.5. Design load cases

The design load cases are obtained for the Pantelleria site (LAT = 37.01° N, LONG = 12.02° E). This is one of the most suitable locations in the Italian sea due to the large amount of wind energy available and the high cost of energy. More details about the chosen site can be found in Cottura et al. (2021).

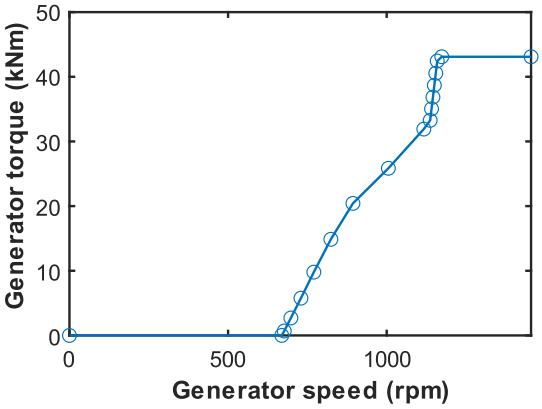

Fig. 9. The speed–torque curve of the generator.

Table 8
Look-up table properties for the aerodynamic loads.

	Min	Max	Step
Wind speed (m/s)	5	25	0.2, 1
Rotor speed steady-state difference (rpm)	−2	2	1
Blade pitch steady-state difference (deg)	−12	12	1

The selected design load cases belong to the Power production condition in which the floating wind turbine is tested under different turbulence models and sea states during operating condition as specified in IEC 61400-3 (IEC, 2019a). However, the design load case considered in this study is limited to DLC 1.1, as we have considered the normal turbulence model and the normal irregular sea state. In this study, we have not considered the modelling of the current, as this is expected to be small in the Mediterranean Sea. Furthermore, we have not investigated the misalignment between waves and wind, which are instead considered with same direction. Extreme conditions and fault conditions are not considered at this stage and needs to be considered in a more detailed design stage where also structural loads and integrity are modelled. Future studies could consider further design load cases, such as DLC 1.6, which also simulates a severe sea state.

The identification of the DLC 1.1 has required to analyse the metaoceanic conditions for Pantelleria. They have been obtained from the ERA5 website (ECMWF, 2022) for the decade 2010–2019, which provides hourly estimates of significant height (H_s), energy period (T_e) and wind speed at reference height (V_0) for a 28 km ×28 km grid. The data from ERA5 are processed in an in-house Python/MATLAB code to elaborate the final triads of

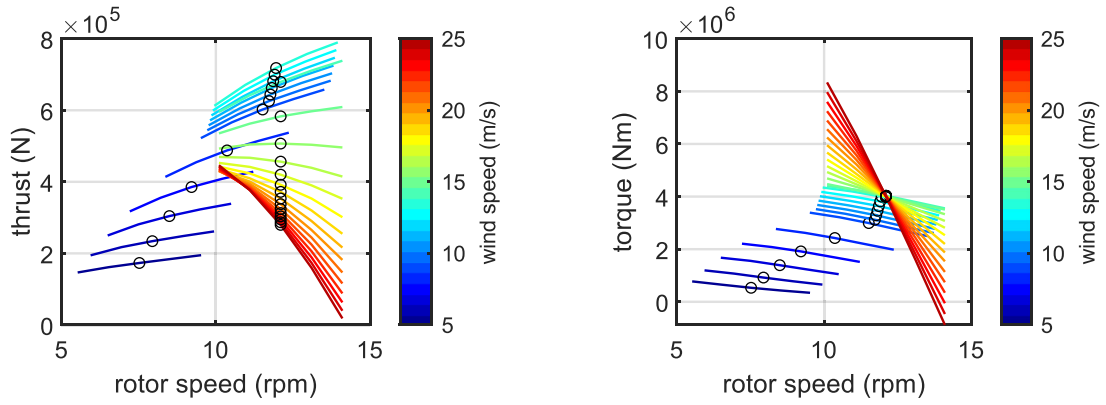

(a) (b)

Fig. 10. Aerodynamic thrust (a) and torque (b) as a function of the rotor speed and wind speed for the steady-state blade pitch. The steady-state conditions are marked as black circles in the figure. (For interpretation of the references to colour in this figure legend, the reader is referred to the web version of this article.)

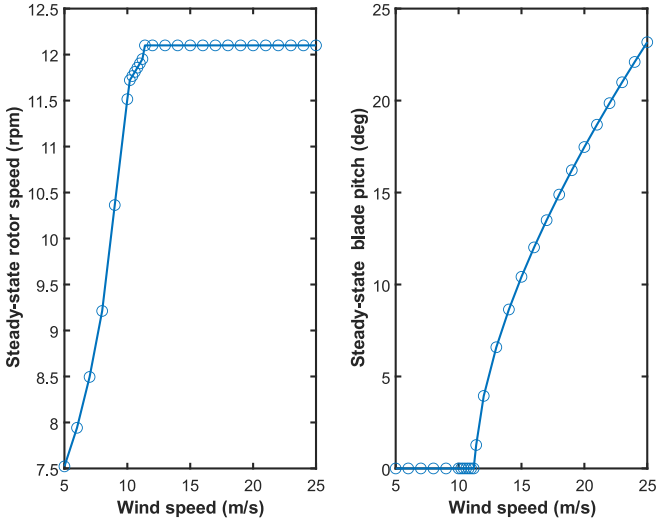

Fig. 11. The steady-states of the rotor speed and blade pitch as a function of the wind speed.

H_s, T_e and V_0 for the time-domain simulations. The original data from ERA5 are classified to reduce the number of triads with an H_s step of 2 m, a T_e step of 1.5s and a V_0 step of 2 m/s. The final triads are then selected so that V_0 is in the operating range. The triplets are also selected to maximise H_s for triads with same T_e and V_0, as only the worst environmental conditions are necessary to check the floating stability of the system. Another triad is added to represent the worst wave conditions and the wind speed for the largest thrust ($H_s = 6$m, a $T_e = 9$s and a $V_0 = 11$ m/s). 46 preliminary triads are finally selected for optimisation, as shown in Fig. 12. All these triplets were tested for 20 different combinations of design parameters of the spar created from a Latin Hypercube sampling of the design space. The added triad was found to be mostly the worst case in terms of stability compared to the other triads in the design space, with an average relative error for pitch and nacelle acceleration of about 2% and 8%, respectively. Therefore, this last triad was chosen for the optimisation design in order to reduce the computational time required for the simulations. The wind is modelled with the power law wind-speed profile and the IEC Kaimal turbulence model (IEC, 2019b). The power law exponent was chosen to be 0.14, as suggested by IEC 61400-3 (IEC, 2019a) for offshore wind. NREL TurbSim software (Jonkman and Buhl, 2006) was chosen to obtain the wind speed turbulent values along a two-dimensional

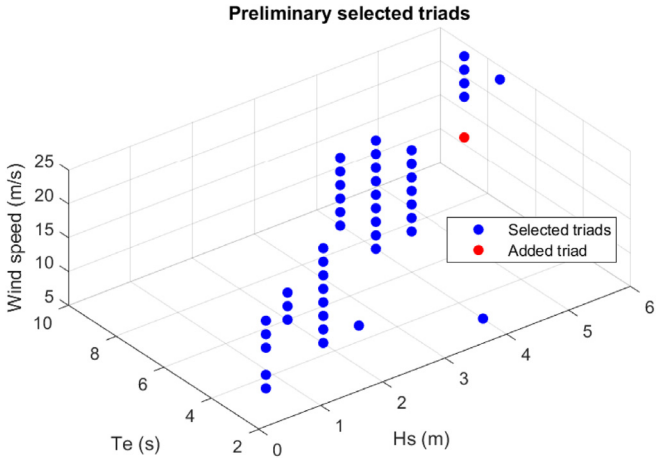

Fig. 12. Preliminary triads selected for the optimisation.

grid of 280 m × 280 m with a discretisation of 17 × 17 points. The time-domain simulation interpolates four points of the wind grid along the blade length. The horizontal hub speed due to

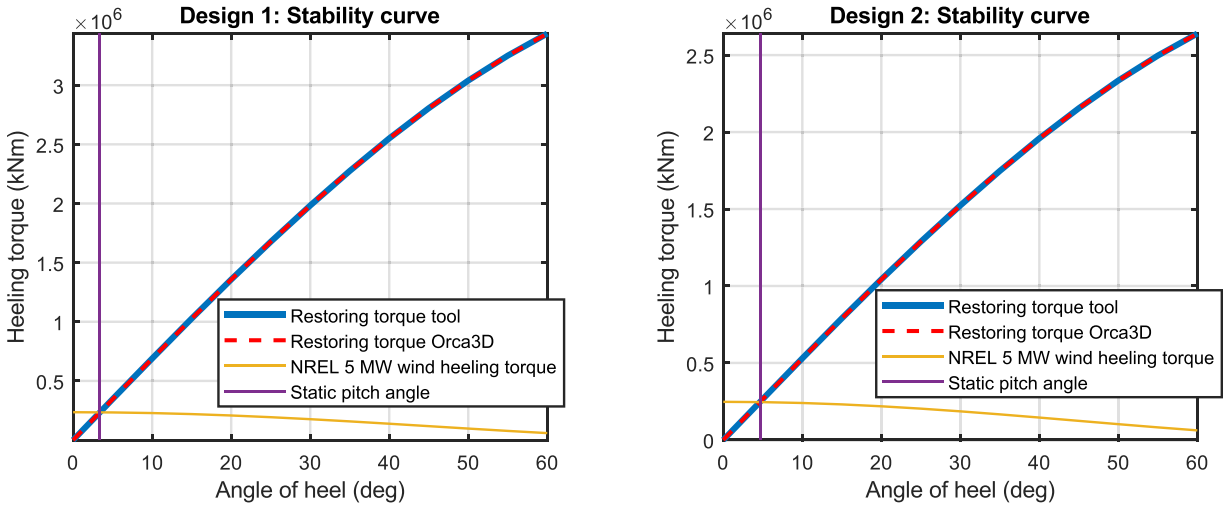

Fig. 13. Verification of the stability curves compared to the commercial software Orca3D for two design solutions of the OC3 spar buoy.

Table 9
Hydrostatic parameters for two different design solutions of the OC3 spar buoy.

	Rspar	Hspar	COG	COB	V	St. angle/ GM stab. curves	St. angle/ GM hydro. stiffness
Design 1	5 m	150 m	[0 0 −116.44] m	[0 0 −83.33] m	11927 m^3	3.39 deg/ 31.99 m	3.55 deg/ 31.89 m
Design 2	4 m	180 m	[0 0 −131.40] m	[0 0 −97.34] m	8897 m^3	4.65 deg/ 31.82 m	4.61 deg/ 31.83 m

surge and pitch oscillation of the platform is also added to the wind speed. The average wind speed for each blade is then determined to compute the aerodynamic loads from the look-up tables described in Section 2.4.3.

3. Results

3.1. Verification of the model

The hydrostatic tool was verified with the commercial software Orca3D (Rhino, 2022). The stability curves obtained with the in-house tool and Orca3D are compared for two design solutions of the OC3 spar buoy. The agreement is excellent, with a relative error in the calculation of the heeling torque less than 0.3%, as shown in Fig. 13. The static pitch angle and metacentric height are calculated using the stability curve. Another alternative is to calculate them using Eqs. (4) and (5) and the hydrostatic stiffness computed in Nemoh. The relative error in the calculation of the static pitch angle and the metacentric height compared to the stability curves is less than 5%. The main hydrostatic parameters of the two solutions are given in Table 9.

The in-house time-domain model MOST was compared with FAST in Cottura et al. (2021). FAST (National Renewable Energy Laboratory, 2021) is a well-known open-source software developed by NREL, which is mainly used for the simulation of offshore wind turbines and was chosen as the reference model for the comparison. The in-house model was able to reproduce the results of FAST quite accurately for the OC3 spar buoy with a relative error of less than 2% in position and output power. However, the in-house code developed in MATLAB required almost twice the simulation time to obtain the results, while an increased computational efficiency was required for the optimisation algorithm. Therefore, MOST was adapted to include look-up tables for the calculation of aerodynamic loads and the mooring. This modification was verified with FAST for the 15 MW TetraSpar floating wind turbine in Sirigu et al. (2022).

Table 10
Optimisation parameters for Hydro1.

	Hydro1Opt1	Hydro1Opt2	Hydro1Opt3
Population GA	20	20	30
Generations GA	7	7	7
Elitism factor surrogate	0.1	0.1	0.1
Fminsearch	10	10	10
Max. stat. pitch constr. (deg)	5	5	5

Table 11
Constraint parameters for each optimisation.

	Dyn1	Dyn2	Dyn3	Dyn4	Hydro1	Hydro2
Stat. pitch constr. (deg)	5	10	5	10	5	10
Dyn. pitch constr. (deg)	5	10	5	10	–	–
Rms acc. constr. (m/s^2)	0.5	0.5	1	1	–	–

3.2. Optimisation convergence

The convergence of the optimisation algorithm is tested for an hydrostatic optimisation (Hydro1) and three different optimisations as described in Table 10. It is assumed that the optimisation is mainly driven by the hydrostatic constraints, so that the convergence test can only be limited to this type of optimisation. Hydro1Opt1 and Hydro1Opt2 have the same number of populations of the genetic algorithm, while Hydro1Opt3 has a larger number. All three optimisations converge to similar results of the objective function (about 12 M€) and therefore the number of generations of Hydro1Opt1 and Hydro1Opt2 is sufficient (Fig. 14).

3.3. Optimisation results

The OC3 design parameters are investigated for different combinations of constraints on the static and dynamic platform pitch constraints and the rms nacelle acceleration constraint. Two values of pitch and acceleration constraints are investigated to understand their influence on the optimal design (see Table 11). Fig. 15 shows the optimisation results for the different simulated optimisation and illustrates the feasible design space with

Table 12
Optimal design parameters for each optimisation.

	Dyn1	Dyn2	Dyn3	Dyn4	Hydro1	Hydro2
Rspar (m)	3.86	3.62	4.65	4.59	4.99	3.85
Hspar (m)	184.65	155.74	138.71	107.46	129.13	141.71
ObjF (M€)	11.68	9.13	11.56	8.96	11.96	9.08
Max static pitch angle (deg)	4.92	9.41	4.98	9.81	4.98	9.91
GM (m)	31.66	20.52	26.29	16.16	24.27	18.35
Steel mass (t)	2959.75	2399.72	2736.66	2171.47	2746.63	2340.13
Ballast mass (t)	5607.10	3855.39	6709.56	4898.30	7433.78	4128.34
Max dynamic pitch angle (deg)	4.70	9.84	4.57	9.03	–	–
Max rms acc. (m/s^2)	0.35	0.35	0.45	0.48	–	–
Mean power (MW)	4.26	4.20	4.26	4.22	–	–

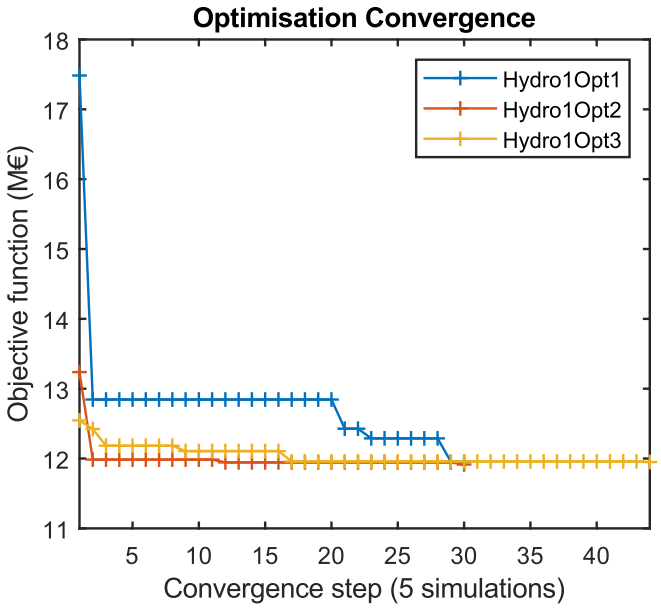

Fig. 14. Convergence results of the Hydro1 optimisation.

the colourmap. The black and the grey dots represent the hydrostatic and dynamic constraints. The optimal design solution is represented with the green dot. The design solutions with same value of the objective function without accounting for the constraints are shown with a green line. The optimal objective function is similar between Dyn1, Dyn3 and Hydro1 and between Dyn2, Dyn4 and Hydro2. In fact, the optimal results are mostly influenced by the static pitch angle constraint. The influence of the dynamic pitch angle constraint is limited to a few cases besides the optimal solution of Dyn2. Short spar configurations are limited by nacelle acceleration constraints for Dyn1 and Dyn2, as moments of inertia and rotational drag are likely to be lower. Dyn3, Dyn4, Hydro1 and Hydro2 instead show that several alternative optimal design solutions could be chosen from those indicated by the green line.

3.4. Optimal configurations

The optimal design solutions from the optimisation are summarised in Table 12. A similar optimal spar radius is obtained from Dyn1 and Dyn2 and from Dyn3 and Dyn4. However, the optimal spar height is shorter for Dyn2 and Dyn4 than for Dyn1 and Dyn3 respectively. In fact, the static pitch angle constraint is less restrictive for Dyn2 and Dyn4 (10 degrees instead of 5 degrees), so smaller and cheaper configurations are feasible. The static pitch angle constraint also has a significant impact on the optimal objective function, which is reduced by about 25% when the static pitch angle constraint is increased from 5 to 10 degrees. The maximum static pitch angles of the design solutions are all next to the static pitch angle constraint for each optimisation case, as minimising structural costs implies the largest possible static pitch angles. The maximum dynamic pitch angle is also determined close to the dynamic pitch constraint and is similar to the maximum static pitch angle. The steel and ballast masses generally differ between the optimal design cases, but the ballast mass is larger than the steel mass in all cases.

Fig. 16 shows the time-domain results for the optimal design cases (Dyn1-Dyn4) and for a chosen time window. The wind and wave elevation refer to the chosen triad for the optimisation described in Section 2.5 ($H_s = 6$ m, a $T_e = 9$ s and a $V_0 = 11$ m/s). Platform pitch and nacelle acceleration show some similarities between Dyn1 and Dyn3 and between Dyn2 and Dyn4. The power produced, on the other hand, is only slightly influenced by the design configuration. Finally, a graphical representation of the optimal design solutions is given in Fig. 17.

4. Discussion

The results of this study show how much the design constraints of optimisation influence the optimal design. The structural cost of the spar is larger with more restrictive constraints, varying by about 25% from the most restrictive to the least restrictive optimal case. The optimal design reduces costs also by two to three times compared to the worst configuration of the design space, making the design optimisation very essential. The static pitch angle constraint is the most important of the optimisation constraints, which emphasises the importance of hydrostatic simulation over dynamic simulation. The rms value of the nacelle acceleration is generally quite low, reaching larger values for smaller spars where inertia and rotational drag are also lower. In fact, the usual operating limits of nacelle acceleration are 20%–30% of the gravitational acceleration (between 1.96 and 2.94 m/s^2) (Leimeister et al., 2020; Suzuki et al., 2011; Huijs et al., 2013), well above the values obtained from the optimal results. It is therefore expected that a fatigue analysis of the rotor blades and tower is likely to be verified.

The optimal design solution of Dyn4 is similar to the OC3 reference spar in Jonkman (2010). In fact, the optimal radius and height of the lower cylinder from this study are 4.6 m and 107.5 m, while in Jonkman (2010) they are 4.7 m and 108 m. The platform mass, considering both the structure and the ballast, is also similar to the reference case (7070 t compared to 7466 t). Some difference with the reference could be related to the choice of the ballast density and the thickness of the platform. The other optimal design solutions have a draft that is quite high compared to the OC3 reference case (120 m) and unrealistic for most sites. The constraint on the draft should depend on the water depth of the site under study. In our study, we considered a water depth of 320 m, which is sufficient for the proposed design solution. However, a draft constraint could be added for optimisation in order to reduce the design space and obtain more feasible solutions for other sites as well.

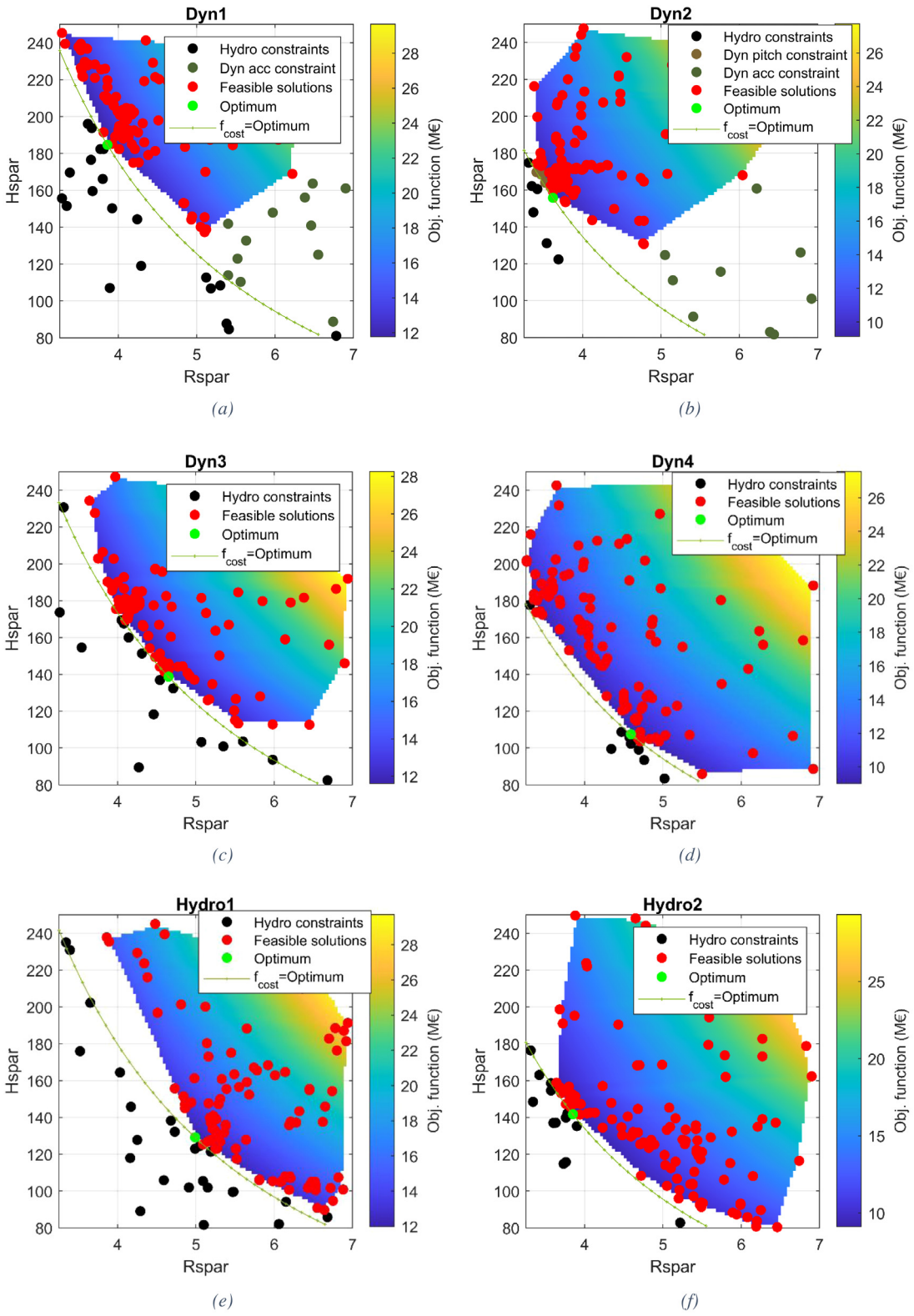

Fig. 15. Optimisation results of the OC3 spar. (For interpretation of the references to colour in this figure legend, the reader is referred to the web version of this article.)

For the optimisations of this study, a critical design load case is determined similar to (Leimeister et al., 2020). However, a different methodology is used to identify the environmental conditions. For example, in this study, the resource data collected from the ERA5 database was used to determine the 46 preliminary triads of H_s, T_e and V_0, while in Leimeister et al. (2020), the DLCs from the IEC (International Electrotechnical Commission) 61400-3 standard were used to define 54 simulations. The dynamic simulations of this study are more limited than in Leimeister et al. (2020), as the yaw misalignment angle between the wind direction and the normal to the rotor plane is not included as well as a current model.

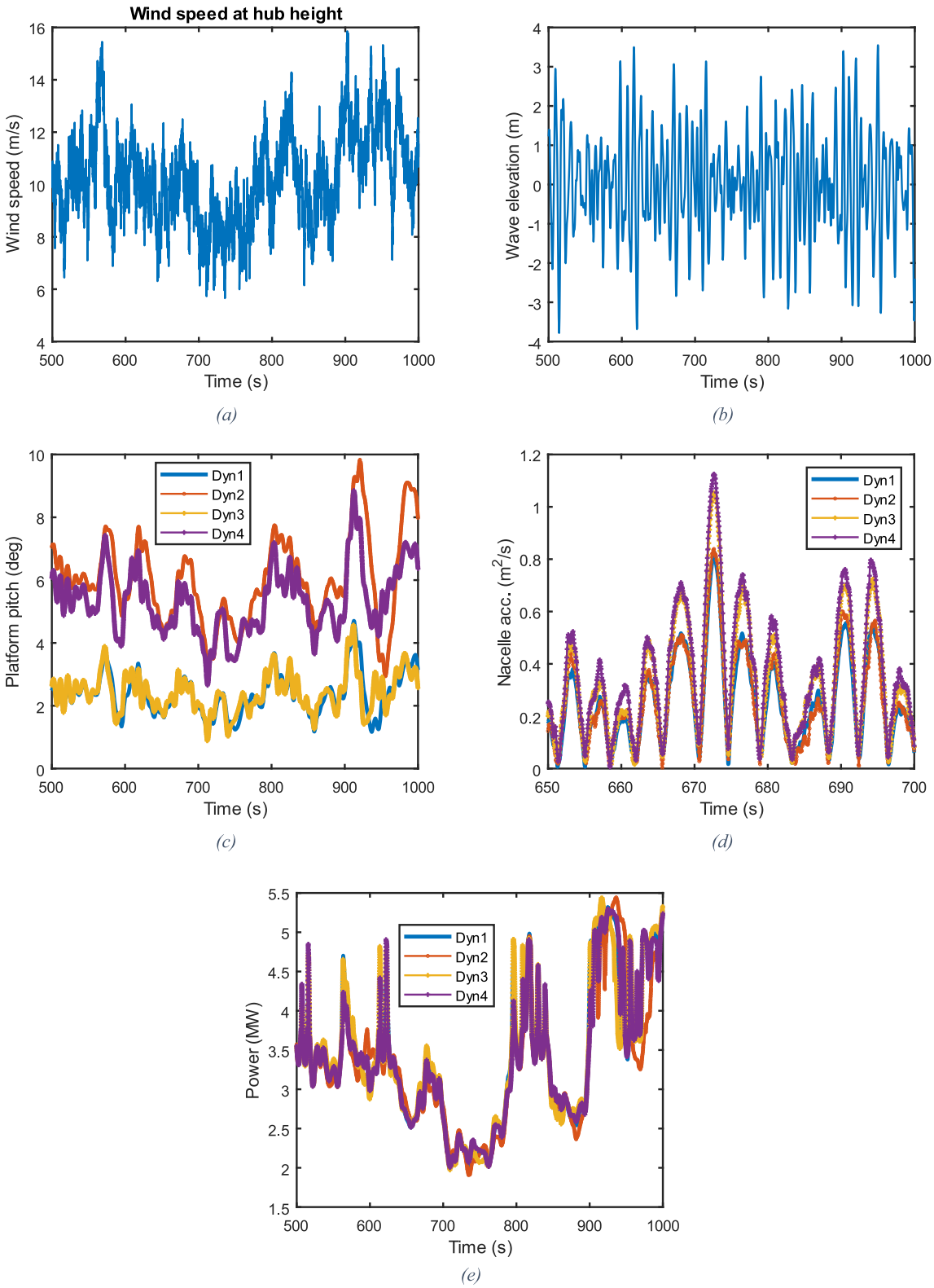

Fig. 16. Time-domain results of wind speed, wave elevation, platform pitch, nacelle acceleration and power for the optimal design configurations.

The structural dynamics of the blades and tower are not considered in the model because the in-house code has not yet developed this feature. However, the elastic behaviour of the structure is expected to have a negligible influence on the system response and can be used for a more accurate computation of fatigue and ultimate loads (Robertson et al., 2017).

The methodology presented in this study, using a hydro-aero-servo model of this study, can also be used to model other floating platforms. Thus, the complexity presented in this study will be similar for other types of platforms, unless the model is extended to include further complexity, e.g. structural modelling of the blades and tower. This work considers only two design variable

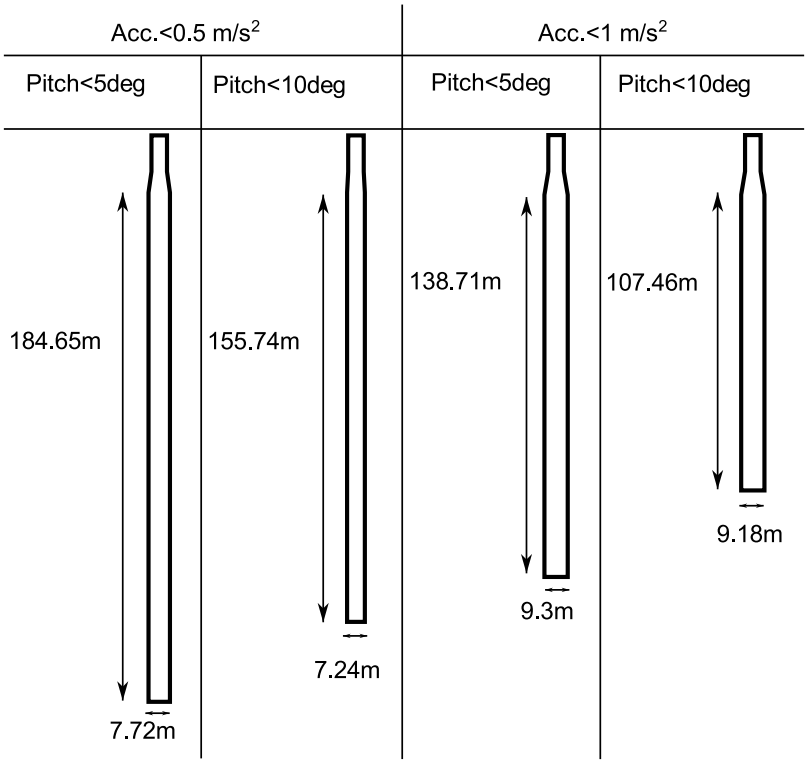

Fig. 17. Optimal configurations.

in the optimisation which is particularly simple and could just consider a parametric study. However, an optimisation algorithm reduces the computational time to achieve an accurate optimal design solution. We therefore still recommend the use of an optimisation algorithm compared to a parametric study. A more complex geometry, such as a semi-submersible platform, is likely to require a larger number of design variables, which increases the simulation time required for optimisation. We assume that we are able to optimise at least 4 design variables without the help of High Performance Computing (HPC) facilities and 6–7 with their help. In fact, the optimisation algorithm can also be used to compute multiple simulations of the individuals of each generation of GA in parallel.

In this study, an in-house numerical tool MOST was preferred over established codes such as OpenFAST for design optimisation. In fact, our tool has some advantages over OpenFAST, such as less computational time due to the use of look-up tables for the calculation of aerodynamic and mooring loads (Sirigu et al., 2022). Another advantage is the flexibility of our tool in modelling complex multi-body systems and hybrid wind-wave systems which could be considered in future works. Indeed, our tool is based on Simscape, which simplifies the numerical modelling of complex multibody systems.

5. Conclusion

This study investigates the optimal design parameters of the OC3 spar buoy in terms of structural costs that minimise the sum of steel and ballast costs. An efficient optimisation algorithm combining the genetic algorithm and the Kriging surrogate model is used to optimise the spar geometry, as each simulation run of the optimisation is fully parametrised as a function of the design parameters. The optimisation is based on MATLAB, coupling together in-house code and open-source software such as Salome-Meca and Nemoh. The Most aero-hydro-servo model is also used to check the platform's dynamic constraints such as dynamic pitch angle and nacelle acceleration. There are two main steps for each simulation run, associated with a hydrostatic module and a dynamic module, which are used to check the design constraints. These two modules are verified with commercial software (Orca3D and Fast) and good convergence of the optimisation algorithm is also observed. A representative design load case for the Pantelleria case study is used for the optimisation, as it is generally the worst condition in terms of stability and nacelle acceleration in the design space. The feasible design solutions are largely restricted by the hydrostatic constraints, while the dynamic constraints have a limited influence. The optimal design changes significantly with the definition of the design constraints, so it is very important to define them accurately. The structure cost varies mainly due to the constraint on the static pitch angle and varies by about 25% between the most expensive and the cheapest optimal configuration.

Further work will investigate the impact of the type of ballast on the optimal design, as cheaper material could lead to better design solutions. An assessment of fatigue should also be included in the model to provide a more accurate estimate of the dynamic constraints associated with fatigue failure. For this purpose, Most will need to include structural modelling to account for these effects. Further work could also include other CAPEX costs in the objective function, such as the cost of the mooring system, as these could be influenced by the hull geometry. Indeed, configurations with larger submerged volumes could determine larger mean drift forces and current loads requiring more expensive station-keeping systems.

CRediT authorship contribution statement

E. Faraggiana: Conceptualization, Methodology, Software, Data curation, Visualization, Formal analysis, Writing – original draft, Writing – review & editing. **M. Sirigu:** Conceptualization, Software, Writing – review & editing. **A. Ghigo:** Conceptualization,

Writing – review & editing. **G. Bracco:** Conceptualization, Supervision, Project administration, Funding acquisition. **G. Mattiazzo:** Supervision, Project administration, Funding acquisition.

Declaration of competing interest

The authors declare that they have no known competing financial interests or personal relationships that could have appeared to influence the work reported in this paper.

Data availability

The authors do not have permission to share data.

References

Ahn, H.-J., Shin, H., 2019. Model test and numerical simulation of OC3 spar type floating offshore wind turbine. Int. J. Nav. Archit. Ocean Eng. 11 (1), 1–10.

Babarit, A., 2017. Nemoh. https://lheea.ec-nantes.fr/logiciels-et-brevets/nemoh-presentation-192863.kjsp.

Cavazzuti, M., 2012. Optimization Methods: from Theory to Design Scientific and Technological Aspects in Mechanics. Springer Science & Business Media.

Codeaster, 2019. Salome-meca. http://www.code-aster.org/spip.php?article303.

Cottura, L., Caradonna, R., Ghigo, A., Novo, R., Bracco, G., Mattiazzo, G., 2021. Dynamic modeling of an offshore floating wind turbine for application in the mediterranean sea. Energies 14 (1), 248.

DNV-GL, 2018. Floating wind turbine structures.

ECMWF, 2022. ERA5. https://www.ecmwf.int/en/forecasts/datasets/reanalysis-datasets/era5. (Accessed 07 February 2022).

Engineering, B.H., 2021. Blue H TLP. https://www.bluehengineering.com/. (Accessed 08 September 2021).

Esteban, M.D., Diez, J.J., López, J.S., Negro, V., 2011. Why offshore wind energy? Renew. Energy 36 (2), 444–450.

EU-OEA, 2010. Oceans of energy. pp. 2010–2050, European ocean energy roadmap.

Faraggiana, E., Chapman, J.C., Williams, A.J., Masters, I., 2020. Genetic based optimisation of the design parameters for an array-on-device orbital motion wave energy converter. Ocean Eng. 218, 108251. http://dx.doi.org/10.1016/j.oceaneng.2020.108251.

Fylling, I., Berthelsen, P.A., 2011. WINDOPT: an optimization tool for floating support structures for deep water wind turbines. In: International Conference on Offshore Mechanics and Arctic Engineering, Vol. 44373. pp. 767–776.

Galván, J., Sánchez-Lara, M.J., Mendikoa, I., Pérez-Morán, G., Nava, V., Rodrıguez-Arias, R., 2018. NAUTILUS-DTU10 MW floating offshore wind turbine at gulf of maine: Public numerical models of an actively ballasted semisubmersible. J. Phys. Conf. Ser. 1102 (1), 12015.

Ghent University, 2022. ooDACE toolbox. http://www.sumo.intec.ugent.be/ooDACE. (Accessed 27 January 2022).

Hall, M., Buckham, B., Crawford, C., 2013. Evolving offshore wind: A genetic algorithm-based support structure optimization framework for floating wind turbines. In: 2013 MTS/IEEE OCEANS-Bergen. pp. 1–10.

Huijs, F., Mikx, J., Savenije, F., de Ridder, E.-J., 2013. Integrated design of floater, mooring and control system for a semi-submersible floating wind turbine. Proc. EWEA Offshore 19, 21.

IEC, 2019a. 61400 -3: Design requirements for floating offshore wind turbines.

IEC, 2019b. 61400-1: Wind energy generation systems. Design requirements.

INNWIND.EU, 2014. Deliverable D4.3.3 – Innovative concepts for floating structures.

James, R., Ros, M.C., 2015. Floating offshore wind: market and technology review. Carbon Trust.

Jonkman, J., 2010. Definition of the floating system for phase IV of OC3.

Jonkman, B.J., Buhl, Jr., M.L., 2006. TurbSim User's Guide.

Jonkman, J., Butterfield, S., Musial, W., Scott, G., 2009. Definition of a 5-MW reference wind turbine for offshore system development.

Karimi, M., Hall, M., Buckham, B., Crawford, C., 2017. A multi-objective design optimization approach for floating offshore wind turbine support structures. J. Ocean Eng. Mar. Energy 3 (1), 69–87.

Kok, S., Sandrock, C., 2009. Locating and characterizing the stationary points of the extended rosenbrock function. Evol. Comput. 17 (3), 437–453.

Lee, J., Shin, S., Kim, S., Kraus, A., Lee, J., 2015. An optimal sub-structure for a TLP-type wind turbine based on neuro-response surface method. J. Mar. Sci. Technol. 20 (4), 604–616.

Leimeister, M., Kolios, A., Collu, M., Thomas, P., 2020. Design optimization of the OC3 phase IV floating spar-buoy, based on global limit states. Ocean Eng. 202, 107186.

Masciola, M., 2018. MAP++ Documentation. NREL Golden, CO, USA.

Masciola, M., Jonkman, J., Robertson, A., 2013. Implementation of a multisegmented, quasi-static cable model.

MathWorks, 2022a. Ode4. https://it.mathworks.com/videos/solving-odes-in-matlab-3-classical-runge-kutta-ode4-117528.html. (Accessed 07 February 2022).

MathWorks, 2022b. Simscape. https://it.mathworks.com/products/simscape.html. (Accessed 25 January 2022).

Myhr, A., Nygaard, T.A., 2012. Load reductions and optimizations on tension-leg-buoy offshore wind turbine platforms.

National Renewable Energy Laboratory, 2021. Fast. https://www.nrel.gov/wind/nwtc/fast.html. (Accessed 07 July 2021).

offshoreWIND.biz, 2017. Statoil floats first hywind Scotland foundations off stord. https://www.offshorewind.biz/2017/05/29/statoil-floats-first-hywind-scotland-foundations-off-stord/. (Accessed 21 January 2022).

QuantDare, 2022. Applying genetic algorithms to define a trading system. https://quantdare.com/ga-to-define-a-trading-system/. (Accessed 27 January 2022).

Renewables Now, 2019. Unitech to take over equinor's Hywind demo off Norway. https://renewablesnow.com/news/unitech-to-take-over-equinors-hywind-demo-off-norway-638882/. (Accessed 21 January 21 2022).

Rhino, 2022. Orca3D. https://orca3d.com/. (Accessed 04 February 2022).

Robertson, A.N., et al., 2017. OC5 project phase II: validation of global loads of the DeepCwind floating semisubmersible wind turbine. Energy Procedia 137, 38–57.

Roddier, D., Cermelli, C., Aubault, A., Weinstein, A., 2010. WindFloat: A floating foundation for offshore wind turbines. J. Renew. Sustain. Energy 2 (3), 33104.

Ruehl, K., Yu, Y.-H., Van Rij, J., Tom, N., 2020. WEC-Sim. https://wec-sim.github.io/WEC-Sim/. (Accessed 30 March 2020).

Sachin Joglekar's blog, 2022. Nelder–Mead optimization. https://codesachin.wordpress.com/2016/01/16/nelder-mead-optimization/. (Accessed 27 January 2022).

Sirigu, M., Faraggiana, E., Ghigo, A., Bracco, G., 2022. Development of a fast simulation model for optimisation of floating offshore wind turbines in Simscape multibody.

Suzuki, K., et al., 2011. Initial design of tension leg platform for offshore wind farm. J. Fluid Sci. Technol. 6 (3), 372–381.

Tethys, 2022. WEC-Sim signature project. https://tethys-engineering.pnnl.gov/signature-projects/wec-sim. (Accessed 05 January 2022).

Yunus, A.C., 2010. Fluid mechanics: Fundamentals and applications (Si units). Tata McGraw Hill Education Private Limited.